# Natural convection in two-layer channel near bottom sludge under the influence of daily temperature fluctuations by the Lattice Boltzmann Method

*Ivan* Volodin[1*], *and Alexey* Alabuzhev[1, 2]

[1]Institute of Continuous Media Mechanics UB RAS, 614013 Perm, Russia
[2]Perm State National Research University, 614990 Perm, Russia

**Abstract.** This study investigates the natural convective flow within an horizontal two-layer system driven by daily temperature fluctuations. The upper part of the layer is free of the porous medium, while the porosity is in the lower part. A homogeneous porosity distribution is assumed along the bottom, mimicking the flow near bottom vegetation or sludge. The Lattice Boltzmann Method is employed to solve the problem. The porous medium is simulated using the representative elementary volume (REV) method. An additional set of distribution functions is implemented to capture temperature distribution. Simulation is performed at constant porosity coefficient and at different Darcy number.

## 1 Introduction

Daily temperature fluctuations have profound consequences for aquatic ecosystems, particularly the flow around bottom vegetation or sludge [1-5]. These changes alter water properties, impacting water movement or impurity transport. It is important, for example, for mixture flow in depositing tank. Dark layer of sludge (slime) is heating during a day and cooling during a night. This heating process causes a thermo-gravitational convection [6-10]. By understanding these complex interactions, we gain insights into vital ecological and environmental processes, including how pollution is transported, how ecosystems respond to change, and how biodiversity is maintained.

The system considered in this paper is a two-layer system, the lower part of which is a porous medium, the upper part is free from a porous medium. One of the most effective methods of studying the evolution of systems is numerical simulation. The approach used in this work is based on the Lattice Boltzmann Method (LBM). In recent decades, it has proven itself to be reliable, efficient and relatively easy to use for considering the dynamics of systems of varying complexity [11-14].

LBM is especially effective for modeling processes occurring in a porous medium. Two main approaches are currently used to model this class of problems: the Pore-Structure (PS) Method and the Representative Elementary Volume (REV) Method. The PS Method requires

* Corresponding author: ivanwolodin@gmail.com

a detailed description of the liquid matrix, including predefined obstacles, where accurately setting distribution function values on these obstacles is essential [12, 13, 15].

In contrast, the REV Method enables the use of empirical models, such as Darcy's law. By expanding the discrete Boltzmann kinetic equation with a small parameter, the Navier-Stokes equation for an incompressible porous medium can be derived (bottom-up approach) [16, 17]. The REV method employs a single set of distribution functions, with porosity and permeability of the medium defined as preset parameters. A comparative analysis of the two methods is provided in [18]. For heterogeneous porous media, the approach detailed in [19] is also applicable.

LBM simulations often introduce an additional set of distribution functions to incorporate temperature distribution. This algorithm has various modifications, including cascaded models, MRT models, and different approaches for handling the source term [11-14, 20-23].

The article is organized as follows. Section 2 briefly discusses the main features of the algorithm used, Section 3 presents the results of the test problem, section 4 discusses the formulation of the main problem, section 5 summarizes the results of the study.

## 2 Numerical model

The idea of the numerical scheme is based on the kinetic Boltzmann equation for the single-particle distribution function $f$ in the phase space of coordinates and momentum.

Evolution equation for the distribution function $f$ is

$$f_i(\boldsymbol{x} + \boldsymbol{c}_i\Delta t, t + \Delta t) = f_i(\boldsymbol{x}, t) - \tau_f^{-1}\left(f_i(\boldsymbol{x}, t) - f_i^{eq}(\boldsymbol{x}, t)\right) + \Delta t\, S_i,$$

where index $i$ represents the discrete mesoscopic velocity, $f^{eq}$ – equilibrium distribution function, $S_i$ – source term, $\boldsymbol{c_i}$ – mesoscopic velocity, $\tau_f$ – relaxation time for $f$, $\Delta t$ – time step.

The presence of the index signifies the restriction of the infinite continuum of mesoscopic velocities to a finite set. The dimensionality of the mesoscopic velocity vector depends on the chosen model: in our simulation set was restricted to 9 (D2Q9 velocity model). The impact of the temperature field to the velocity distribution is performed through the source term.

Additional set of distribution functions ($g$ and $g^{eq}$) is introduced to handle the temperature fluctuations. The evolution equation for this set has the similar form:

$$g_i(\boldsymbol{x} + \boldsymbol{c}_i\Delta t, t + \Delta t) = g_i(\boldsymbol{x}, t) - \tau_g^{-1}\left(g_i(\boldsymbol{x}, t) - g_i^{eq}(\boldsymbol{x}, t)\right)\Delta t,$$

where $\tau_g$ is relaxation time for $g$.

The macroscopic field values are governed by the following equations:

$$\rho(\boldsymbol{x}, t) = \sum_{i=1}^{N} f_i,$$

$$\boldsymbol{u}(\boldsymbol{x}, t) = \frac{1}{\rho(\boldsymbol{x}, t)}\sum_{i=1}^{N} \boldsymbol{c}_i f_i + \frac{\Delta t}{2}\boldsymbol{F}.$$

Here $\boldsymbol{u}$ stands for temporary velocity, $\boldsymbol{F}$ – external force. Medium force resistance ought to be included in the algorithm through the genuine velocity calculation [see e.g. 18]:

$$\boldsymbol{v} = \frac{\boldsymbol{u}}{L_0 + \sqrt{L_0^2 + L_1|\boldsymbol{u}|}},$$

where $L_0$ and $L_1$ are two constant parameters:

$$L_0 = \frac{1}{2}\left(1 + \varepsilon\frac{\Delta t}{2}\frac{\nu}{K}\right),$$

$$L_1 = \varepsilon\frac{\Delta t}{2}\frac{F_\varepsilon}{\sqrt{K}},$$

where $\varepsilon = {V_{pore}}/{V_{total}}$ is the porosity coefficient determined by the ratio of the pore volume to the total volume, $K$ – permeability coefficient, $\nu$ – medium viscosity and $F_\varepsilon = {1.75}/{\sqrt{150\varepsilon^3}}$.

As previously stated, the temperature distributions and velocity distributions are interconnected through the source term $S_i$. In our simulation it has the following form:

$$S_i = w_i\rho\left(1 - \frac{1}{2\tau_f}\right)\left[\frac{\boldsymbol{c_i F}}{c_s^2} + \frac{\boldsymbol{vF}:(\boldsymbol{c_i c_i} - c_s^2\boldsymbol{I})}{\varepsilon c_s^4}\right],$$

where $w_i$ is the contribution of the mesoscopic velocities, normalized by 1, $c_S = 1/\sqrt{3}$ – dimensionilized sound speed, $\boldsymbol{I}$ – unit tensor, $\boldsymbol{F}$ includes both gravity and beyonce force.

Reference [11-14] provides a detailed explanation of the equilibrium distribution functions view, the relationship between temperature coefficients, and the algorithm itself.

The algorithm was implemented using custom C++ code. Visualization of the results was achieved using Python3.11 with the matplotlib and numpy libraries.

## 3 Verification test

As a benchmark problem for our model, consider a square cavity with solid boundaries (no-slip conditions for the function $f$) subjected to a horizontal negative temperature gradient. A no-threshold convective movement arises in this case. The top and bottom walls are adiabatic. The porous media occupies the half of the computational cavity (Fig. 1).

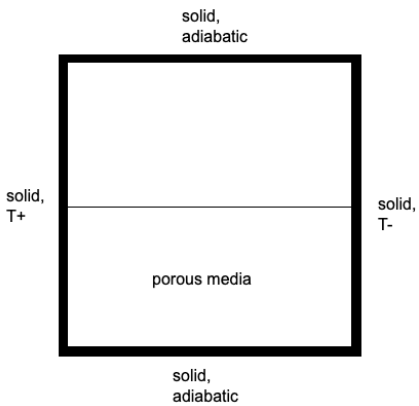


**Fig. 1.** Sketch of the benchmark problem

Considering this problem setup, we investigated it using the following parameters: Rayleigh number $Ra = 10^6$ , Prandtl number $Pr = 7.1$, Darcy number $Da = 2.1 \cdot 10^{-5}$, porosity coefficient $\varepsilon = 0.9$. The grid size is 200x200 and the result of the simulation is shown in Fig. 2.

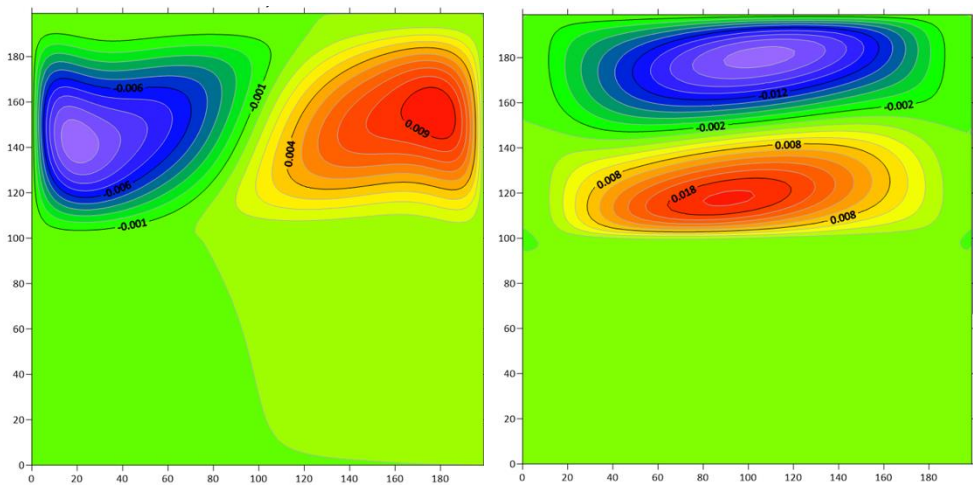


a) b)

**Fig. 2.** Instantaneous isolines of the vertical velocity (a) and longitudinal velocity (b). $Ra = 10^6$, $Da = 2.1 \cdot 10^{-5}$, $Pr = 7.1$, $\varepsilon = 0.9$

To provide comparison with the numerical experiments of other researchers, we examined this problem using the following parameters: $Ra = 10^3$, $\varepsilon = 0.9, Da \simeq 10^{-2}$. The result is depicted in Fig. 3.

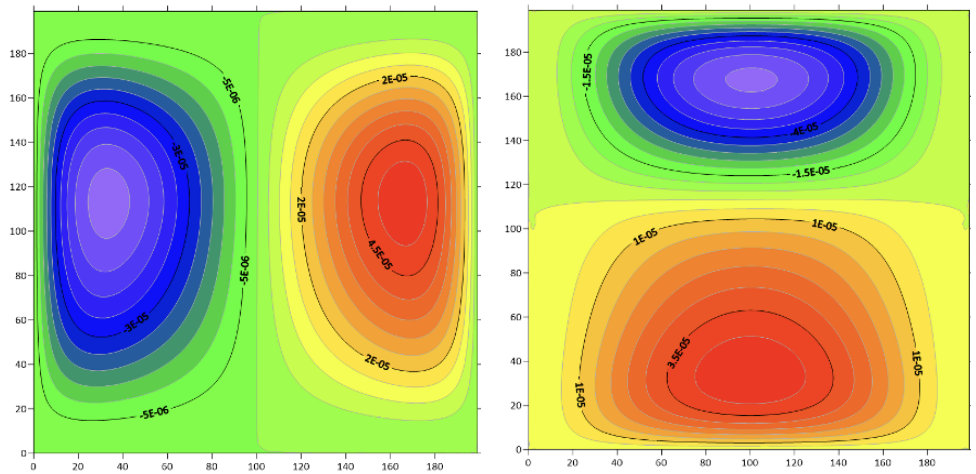


a) b)

**Fig. 3.** Instantaneous isolines of the vertical velocity (a) and longitudinal velocity (b). $Ra = 10^3$, $Da \simeq 10^{-2}$, $Pr = 7.1$, $\varepsilon = 0.9$

As shown by the calculations results, decreasing the Rayleigh number leads to a reduction of the flow intensity. Increasing the Darcy number (and consequently increasing the permeability coefficient $K$) intensifies the flow within the porous medium.

The obtained results were found to be qualitatively similar to those presented in [21].

## 4 Flow simulation under the temperature fluctuations

Let us consider a flow in a two-layer channel, where the porous medium occupies the whole lower part of the domain (up to $y = {}^{N_y}/_{5}$ nodes), and the motion is driven by heating the bottom wall with a prescribed oscillatory period (Fig. 4). Consequently, the dimensionless top temperature is 0.1, bottom temperature varies in range from 0.1 to 1.1. It allows to simulate the diurnal temperature variational.

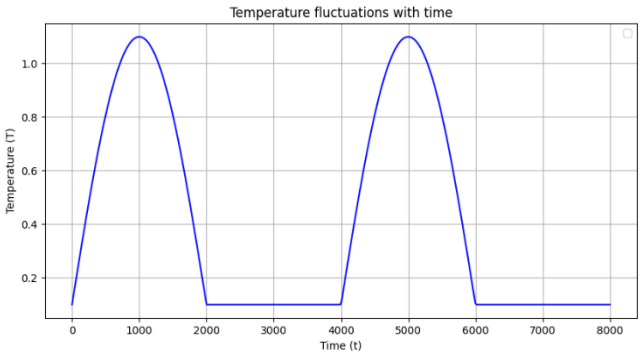


**Fig. 4.** Temperature profile at the bottom wall of the computational domain

The boundary conditions of the problem correspond to an infinite layer: periodic conditions are applied to the side walls, the bottom wall is solid, and the top wall has a free-slip condition with a constant temperature. The temperature value at the bottom of the domain is shown in Fig. 4.

Characteristic viscous attenuation time $t_\nu = {}^{N_y^2}/_{\nu}$ is comparable to the period of temperature fluctuations at the bottom of the computational domain. The problem was solved on a 100x100 grid, dimensionless parameters are: $Ra = 10^3$, $Da = 2 \cdot 10^{-4}$.

Apparently, with this problem setup, it is impossible to reach a steady-state flow condition; therefore, we will present the velocity components of the convective flow and the velocity field oscillations in the center of the porous medium ($x = {}^{N_x}/_{2}, y = {}^{N_y}/_{10}$) and in a region away from it ($x = {}^{N_x}/_{2}, y = {}^{N_y}/_{2}$).

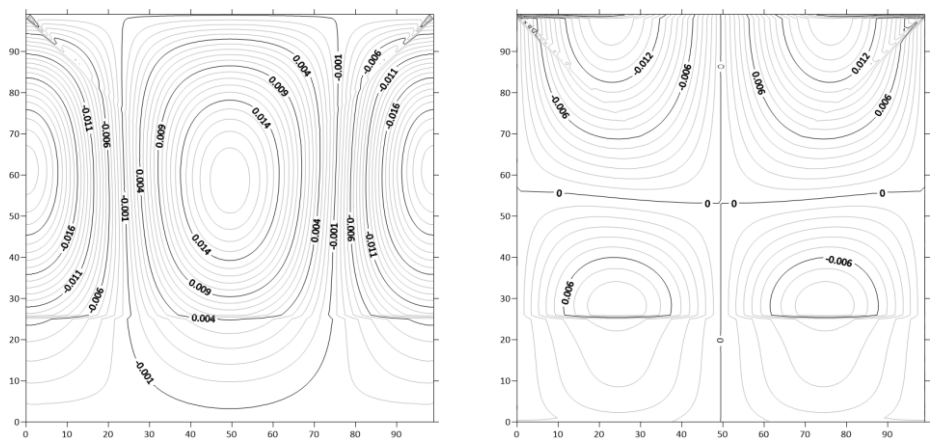

a) b)

**Fig. 5.** Vertical velocity component (a) and longitudinal velocity component (b) of the flow

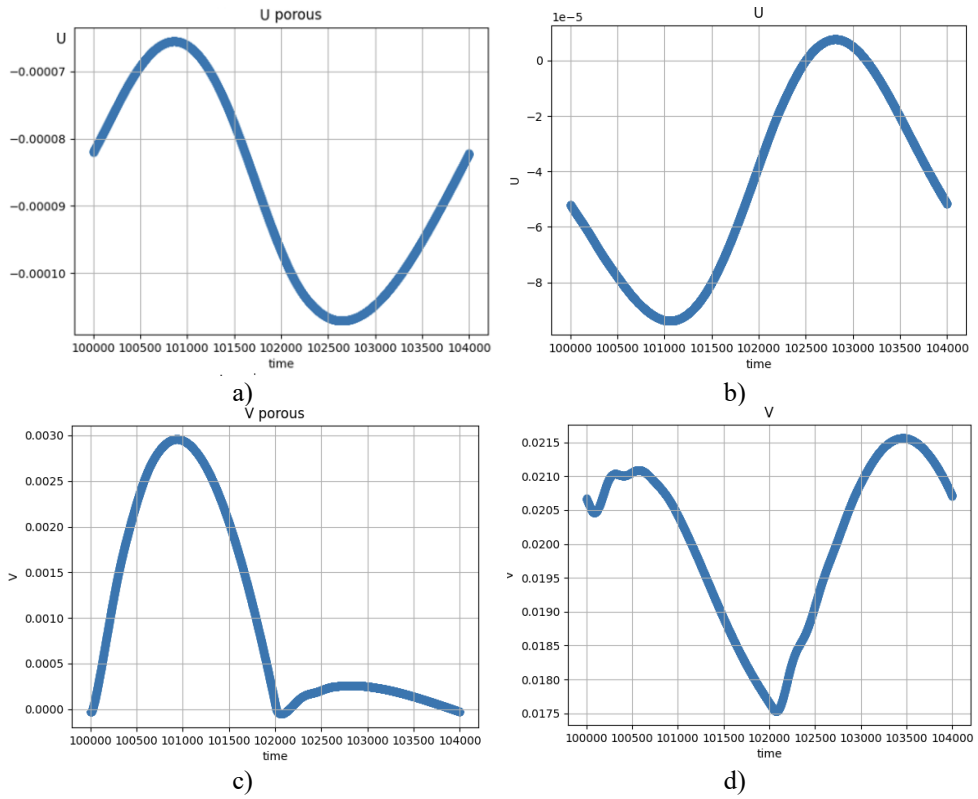


**Fig. 6.** Pulsating of the velocity components. Longitudinal and vertical component in porous media (a, c) and in liquid layer (b, d)

As can be seen in Fig. 5, a low Darcy number results in very weak flow intensity within the porous medium. The presence of periodicity in the developed flow (Fig. 6) allows us to assess the influence of temperature oscillations on the velocity field distribution.

## 5 Acknowledgements

This work was financial supported by the Russian Science Foundation (project No. 24-21-00379)

## References

1. M. Baure, L. Eichinger, P. Elsass, W. Kloppmann, G. Wirsing, *Int. J. Earth Sci.* **94**, 565-579 (2005)
2. M. G. Wells, J. S. Wettlaufer, *J. Fluid Mech.* **572**, 37-58 (2007)
3. E. Khayrulina, N. Maksimovich, *Mine Water Environ.* **37**, 595-603 (2018)
4. E. Khayrulina, A. Bogush, L. Novoselova, N. Mitrakova, *Forests* **12**, 321 (2021)
5. B. S. Maryshev, Y. N. Parshakova, A. O. Ivantsov, N. A. Zubova, *Computational Continuum Mechanics* **15**, 209–222 (2022)

6. Y. N. Parshakova, M. V. Viskov, R. I. Kataev, N. N. Kartavykh, *Computational Continuum Mechanics* **17**, 151-159 (2024)
7. D. V. Lyubimov, *J Appl Mech Tech Phys* **16**, 257–261 (1975)
8. S. C. Hirata, B. Goyeau, D. Gobin, *Transp Porous Med* **78**, 525–536 (2009).
9. D. A. Nield, A. Bejan, Convection in Porous Media (Springer, Switzerland, 2017)
10. E. A. Kolchanova, N. V. Kolchanov, *Int. J. Heat Mass Transf.* **106**. 47-60 (2017)
11. M.C. Sukop, D.T. Thorne, Lattice Boltzmann Modeling: An Introduction for Geoscientists and Engineers (Springer, Berlin, 2007)
12. S. Succi, The Lattice Boltzmann Equation: For Complex States of Flowing Matter (Oxford University Press, 2018)
13. T. Krüger, H. Kusumaatmaja, A. Kuzmin, O. Shardt, G. Silva, E. Viggen, The Lattice Boltzmann Method (Springer, Berlin, 2017)
14. Mohamad, Lattice Boltzmann Method. Fundamentals and Engineering Applications with Computer Codes (Springer Berlin, 2011)
15. S. Succi, E. Foti, F. Higuera, *Europhys. Lett.* **10**, 433–438 (1989)
16. Z. Guo, T. Zhao, *Phys. Rev. E* **66**, 036304 (2002)
17. Z. Guo, C. Zheng, B. Shi, *Phys. Rev. E* **65**, 046308 (2002)
18. D. D'Orazio, A. Karimipour, R. Ranjbarzadeh, *Energies* (2023)
19. M. P. Lautenschlaeger, J. Weinmiller, B. Kellers, T. Danner, A. Latz, *Adv. Water Resour.* **170**, 104320 (2022)
20. A. Zarghami, S. Di Francesco, C. Biscarini, *Int. J. Mod. Phys*. C 25, 1350086 (2014).
21. S. Hassan, T. Himika, M.M. Molla, F. Hasan, *Comput. Eng. Phys. Model.* 2(4), 38–57 (2019).
22. Q. Liu, Y.-L. He, *Physica A* **45**, 742–753 (2017).
23. Q. Liu, X.-B. Feng, Y.-L. He, C.-W. Lu, Q.-H. Gu, *Appl. Therm. Eng.* **152**, 319–337 (2019).